Implementation of Dual Reciprocity Boundary Element Method for Heat Conduction Problems in Anisotropic Solid

A. A. Nithi Pramesti, Imam Solekhudin*, Moh. Ivan Azis

***Abstract*—In this paper, some time-dependent heat conduction problems in anisotropic thin plates are considered. To study the problems, the governing equations of the problems are transformed into Helmholtz-type equations. The Helmholtz-type equations with respect to transformed boundary conditions are solved numerically using Dual Reciprocity Boundary Element Method (DRBEM). The method is tested using several problems involving time-dependent heat conduction in anisotropic thin plates. Two of the problems are with analytical solution, and the other problem is with unknown analytical solution. For problems with analytical solution, numerical results obtained using the method have a good accuracy. Moreover, the method is implemented to examine variation of temperature in the anisotropic thin plates as time increases.**

***Index Terms*—Time-dependent heat equation, heat distribution, anisotropic solid, Laplace transform, DRBEM.**

I. Introduction

HEAT conduction problems in anisotropic materials have been an attractive matters for researchers. A number of researchers have studied these problems. Such researchers are Paddock and Eesley [1], Capinski et. al. [2], Norris et. al. [3], and Huxtable et. al. [4]. Paddock and Eesley investigated transient thermoreflectance from thin metal films [1]. Thermal conductivity measurements using a picosecond optical pump and probe technique was examined by Capinski et. al. [2]. Norris et. al. conducted femtosecond pump probe technique examination of some materials [3]. Huxtable et. al. studied thermal conductivity imaging at micrometre scale [4]. Most of these study are experimental studies.

One way to study heat conduction in anisotropic materials is through mathematical modelling. However, generally, the resulting mathematical model may not be solved analytically. Hence, in this paper we employ a numerical method to solve the model. The numerical method used is a type of Boundary Element Methods (BEM), which is known as Dual Reciprocity Boundary Element Methods (DRBEM). One of the advantages of these methods is their ability to reduce the dimension of the problem. The problems considered in this paper, which are time-dependent with two-dimensional space problems, may be reduced into one-dimensional problems. Boundary element methods have been employed by numerous researchers in their studies. Clements and Lobo [5], Solekhudin [6], and Munadi et. al. [7], [8] employed boundary element techniques to solve problems involving water infiltration into homogeneous soils. Ashar and Solekhudin [9] used the method for simulating pollutant spread from a point source in a river.

The problems considered by the researchers are in homogeneous materials. Some of studies employing boundary element techniques for solving problems in nonhomogeneous materials have been also conducted by some researchers. Solekhudin used the method for solving infiltration problems into layered soils [10]. Ang and Clements used the method to solve nonlinear heat equation in nonhomogeneous anisotropic materials [11]. Azis et. al. [12] solved problems in anisotropic functionally graded materials using the method. In this paper, a DRBEM is employed to solve time-dependent heat equations in anisotropic materials. The method is tested to solve two problems with analytical solutions, in order to investigate accuracy of the method. In addition, the method is applied to solve a time-dependent heat equation with unknown analytical solution. Numerical solutions are presented to determine the dynamics of changes in temperature distribution in the anisotropic materials.

Manuscript received June 20, 2021; revised December 27, 2021.

A. A. Nithi Pramesti was a student at Department of Mathematics, Faculty of Mathematics and Natural Sciences, Universitas Gadjah Mada, Yogyakarta, INDONESIA.

*Corresponding author. Imam Solekhudin is an Associate Professor at the Department of Mathematics, Universitas Gadjah Mada, Yogyakarta, INDONESIA e-mail: imams@ugm.ac.id.

Moh. Ivan Azis is a Professor at the Department of Mathematics, Faculty of Mathematics and Natural Sciences, Hasanuddin University, Makassar, INDONESIA. E-mail: ivan@unhas.ac.id

II. Problem Formulation and Basic Equations

In this section, mathematical models of problems involving time-dependent heat equations in anisotropic materials are presented. For the convenience of readers, a brief derivation from a time-dependent heat equation into a Helmholtz-type equation is presented. We consider a non-homogeneous anisotropic solid on the Ox_1x_2 plane. Heat conduction in the solid material is modelled as

$$\sum_{i=1}^{2}\sum_{j=1}^{2}\frac{\partial}{\partial x_i}\left(k_{ij}\frac{\partial T}{\partial x_j}\right)+g=\rho C\frac{\partial T}{\partial t}, \tag{1}$$

where $T(x_1,x_2,t)$ is the temperature at point (x_1,x_2) at time $t>0$, k_{ij} are the thermal conductivity coefficients that are considered to be the components of a conductivity matrix

$$\bar{\bar{k}}=\begin{bmatrix}k_{11} & k_{12}\\ k_{21} & k_{22}\end{bmatrix}, \tag{2}$$

and g, ρ, C are respectively the internal heat generation, the density, and the specific heat capacity of the materials. Here, the thermal conductivity coefficients satisfy $k_{ij}=k_{ji}$ and $k_{ii}k_{jj}>kij^2$, for $i\neq j$.

If the thermal conductivity coefficients are constants, Equation (1) can be written as

$$\sum_{i=1}^{2}\sum_{j=1}^{2} k_{ij}\frac{\partial^2 T}{\partial x_i x_j} + g = \rho C\frac{\partial T}{\partial t}. \tag{3}$$

The problem of interest here is solving Equation (3) in a two dimensional region R bounded by a simple closed curve B subject to initial condition $T(x_1, x_2, 0) = T_0(x_1, x_2)$ and boundary conditions

$$T(x_1, x_2, t) = f_1(x_1, x_2) \text{ for } (x_1, x_2) \in B_1 \text{ and } t > 0, \tag{4}$$

$$\sum_{i=1}^{2}\sum_{j=1}^{2} k_{ij} n_i \frac{\partial T}{\partial x_j} = f_2(x_1, x_2) \text{ for } (x_1, x_2) \in B_2 \text{ and } t > 0, \tag{5}$$

where T_0, f_1 and f_2 are suitably prescribed functions, B_1 and B_2 are non-intersecting curves such that $B_1 \cup B_2 = B$ and $[n_1, n_2]$ is the unit normal vector pointing out curve B.

Since the conductivity matrix (2) is symmetric, it is possible to obtain a new coordinate system of rectangular coordinates $Ox_1'x_2'$, where

$$\begin{bmatrix} x_1' \\ x_2' \end{bmatrix} \begin{bmatrix} \cos\theta & \sin\theta \\ -\sin\theta & \cos\theta \end{bmatrix} = \begin{bmatrix} x_1 \\ x_2 \end{bmatrix}, \tag{6}$$

for a rotation angle θ, such that $\bar{\bar{k}}$ is transformed into

$$\bar{\bar{k}}' = \begin{bmatrix} k_1 & 0 \\ 0 & k_2 \end{bmatrix}. \tag{7}$$

Quantity k_1 and k_2 are called the *principal conductivities* along the principal coordinates axes x_1' and x_2', respectively. Using the coordinate system $Ox_1'x_2'$, Equation (3) becomes

$$\sum_{i=1}^{2} k_i \frac{\partial^2 T}{\partial {x_i'}^2} + g = \rho C\frac{\partial T}{\partial t}, \tag{8}$$

which is the equation of heat conduction in orthotropic solid.

The heat conduction equation for an orthotropic solid (8) can be transformed to a standard heat conduction equation for an isotropic solid using new coordinate system OX_1X_2, where X_1 and X_2 are defined as

$$X_1 = x_1'\left(\frac{k}{k_1}\right)^{\frac{1}{2}} \quad \text{and} \quad X_2 = x_2'\left(\frac{k}{k_2}\right)^{\frac{1}{2}}, \tag{9}$$

where k is a reference conductivity, satisfying

$$k = (k_1 k_2)^{\frac{1}{2}}. \tag{10}$$

Now heat equation (8) becomes

$$k\sum_{i=1}^{2} \frac{\partial^2 T}{\partial X_i^2} + g = \rho C\frac{\partial T}{\partial t}, \tag{11}$$

which is the equation of heat conduction in isotropic solid.

Using Laplace transform

$$\overline{T} = \int_0^\infty T(x, y, t)e^{-st}dt, \tag{12}$$

equation (11) can be written as

$$\frac{\partial^2 \overline{T}}{\partial {X_1}^2} + \frac{\partial^2 \overline{T}}{\partial {X_2}^2} - \left(\frac{\rho C s}{k}\right)\overline{T} = \frac{-\rho C T_0 - \overline{g}}{k}, \tag{13}$$

where $\overline{T}$ and $\overline{g}$ is the Laplace transformations of T and g respectively. Equation (13) is a Helmholtz-type equation.

Applying Transformations 6, 7, and 9, Boundary conditions (4) and (5) can be transform into

$$\begin{aligned}\overline{T} =& \overline{u}\left(X_1\left(\frac{k_1}{k}\right)^{1/2}\cos\theta - X_2\left(\frac{k_2}{k}\right)^{1/2}\sin\theta,\right.\\ & \left. X_1\left(\frac{k_1}{k}\right)^{1/2}\sin\theta + X_2\left(\frac{k_2}{k}\right)^{1/2}\cos\theta, s\right)\\ & \text{for } (X_1, X_2) \in B_1,\end{aligned} \tag{14}$$

$$\begin{aligned}\frac{\partial \overline{T}}{\partial n} =& \overline{v}\left(X_1\left(\frac{k_1}{k}\right)^{1/2}\cos\theta - X_2\left(\frac{k_2}{k}\right)^{1/2}\sin\theta,\right.\\ & \left. X_1\left(\frac{k_1}{k}\right)^{1/2}\sin\theta + X_2\left(\frac{k_2}{k}\right)^{1/2}\cos\theta, s\right)\\ & \times\left(\frac{\sqrt{\frac{k_1}{k}\left(\hat{X}_1\right)^2 + \frac{k_2}{k}\left(\hat{X}_2\right)^2}}{k\sqrt{\left(\hat{X}_1\right)^2 + \left(\hat{X}_2\right)^2}}\right)\\ & \text{for } (X_1, X_2) \in B_2.\end{aligned} \tag{15}$$

To solve Equation (13) using DRBEM, we express the solution in the form of an integral equation

$$\begin{aligned}\lambda(\xi,\eta)\overline{T}(\xi,\eta,s) =& \int_B \left[\overline{T}(X_1, X_2, s)\frac{\partial \Phi(X_1, X_2; \xi, \eta)}{\partial n}\right.\\ & \left. - \Phi(X_1, X_2; \xi, \eta)\frac{\partial \overline{T}(X_1, X_2, s)}{\partial n}\right] ds\\ & + \iint_R \Phi(X_1, X_2; \xi, \eta)\big[G(X_1, X_2, s, k)\\ & + \mathcal{A}(s, k)\overline{T}(X_1, X_2, s)\big] dX_1 dX_2,\end{aligned} \tag{16}$$

where

$$\lambda(\xi,\eta) = \begin{cases} \frac{1}{2}, & \text{if } (\xi,\eta) \text{ on smooth part of } B \\ 1, & \text{if } (\xi,\eta) \in R \end{cases}, \tag{17}$$

$$\Phi(x, y; \xi, \eta) = \frac{1}{4\pi}\ln[(x-\xi)^2 + (y-\eta)^2], \tag{18}$$

$$G(a^{(j)}, b^{(j)}, s, k) = \frac{-\rho C T_0(a^{(j)}, b^{(j)}) - \overline{g}(a^{(j)}, b^{(j)}, s)}{k}, \tag{19}$$

and

$$\mathcal{A}(s, k) = -\frac{\rho C s}{k}. \tag{20}$$

Equation (16) is then solved numerically by recasting the equation into a system of linear algebraic equations as those in [13], [14].

Numerical solutions of $\overline{T}$ obtained are in Laplace domain. Hence, an inverse Laplace transform is needed. Here, we use the Stehfest formula [15] formulated as

$$T(X_1, X_2, t) \simeq \frac{\ln(2)}{t}\sum_{p=1}^{2P} K_p \overline{T}(X_1, X_2, s_p), \tag{21}$$

where

$$s_p = p\frac{\ln(2)}{t}, \tag{22}$$

$$K_p = \sum_{m=\frac{p+1}{2}}^{\min(p,P)} \frac{m^P(2m)!}{(P-m)!m!(m-1)!(p-m)!(2m-p)!}, \times (-1)^{p+P} \tag{23}$$

where P is a positive integer. To obtain a good accuracy and efficiency of computational times, we take $P = 3$.

III. Specific Problems

The method presented in the preceding section is tested using three problems. The first two problems are used to test the accuracy of the method. The third problem, which may not be solved analytically, is solved to present the behavior of heat distribution in an anisotropic solid.

The three problems have the same domain, which is illustrated in Figure 1.

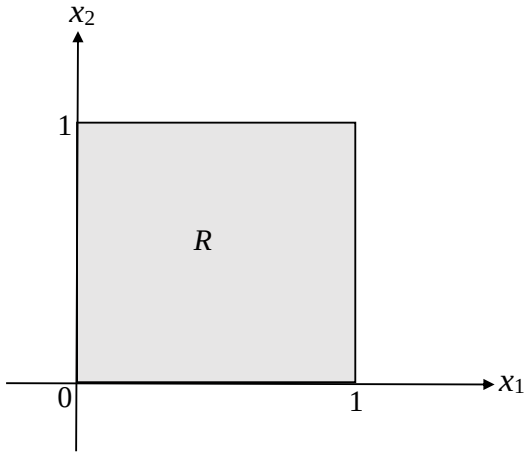

Fig. 1: Domain of Problem 1, Problem 2, and Problem 3.

The boundary of the domain, B, is notated as $B = B_1 \cup B_2 \cup B_3 \cup B_4$, where

$$B_1 = \{(x_1, x_2) \in \mathbb{R} |\, x_1 = 0, 0 \le x_2 \le 1\}, \tag{24}$$
$$B_2 = \{(x_1, x_2) \in \mathbb{R} |\, x_1 = 1, 0 \le x_2 \le 1\}, \tag{25}$$
$$B_3 = \{(x_1, x_2) \in \mathbb{R} | 0 < x_1 < 1, x_2 = 0\}, \tag{26}$$
$$B_4 = \{(x_1, x_2) \in \mathbb{R} | 0 < x_1 < 1, x_2 = 1\}. \tag{27}$$

A. Problem 1

In this problem, We consider an anisotropic square thin plate region R, where

$$R = \{(x_1, x_2) \in \mathbb{R} |\, 0 < x_1 < 1, 0 < x_2 < 1\}.$$

The heat equation on the thin plate is

$$\frac{\partial T}{\partial t} = 9\frac{\partial^2 T}{\partial x_1^2} + 3\frac{\partial^2 T}{\partial x_2^2} + 4\frac{\partial^2 T}{\partial x_1 \partial x_2} + x_1^2 - 180x_1 - 480x_2 - 18t, \tag{28}$$

subject to initial boundary conditions

$$T(x_1, x_2, 0) = 30x_1x_2^2 + 10, \tag{29}$$
$$T(x_1, x_2, t) = 10, \text{ for } (x_1, x_2) \in B_1 \text{ and } t > 0, \tag{30}$$
$$T(x_2, x_2, t) = t + 30x_2^2 + 10, \text{ for } (x_1, x_2) \in B_2 \text{ and } t > 0, \tag{31}$$
$$\sum_{i=1}^{2}\sum_{j=1}^{2} k_{ij}\frac{\partial T}{\partial x_i}n_{x_j} = -18tx_1, \text{ for } (x_1, x_2) \in B_3 \text{ and } t > 0, \tag{32}$$
$$\sum_{i=1}^{2}\sum_{j=1}^{2} k_{ij}\frac{\partial T}{\partial x_i}n_{x_j} = 18tx_1 + 180x_1 + 270, \text{ for } (x_1, x_2) \in B_4 \text{ and } t > 0. \tag{33}$$

The analytic solution of the problem is

$$T(x_1, x_2, t) = tx_1^2 + 30x_1x_2^2 + 10. \tag{34}$$

To implement DRBEM, Heat equation (28) is transformed into a Helmholtz-type equation using Transformation (6), Transformation (9) and Laplace transform. The resulted equation is

$$\frac{\partial^2 \overline{T}}{\partial {X_1}^2} + \frac{\partial^2 \overline{T}}{\partial {X_2}^2} - \left(\frac{s}{k}\right)\overline{T} = \frac{-30(1.628X_1 - 0.245X_2)(0.814X_1 + 0.491X_2)^2}{k} - \frac{1}{sk}\Big((1.628X_1 - 0.245X_2)^2 - 180(1.628X_1 - 0.245X_2) - 480(0.814X_1 + 0.491X_2) - \frac{18}{s}\Big). \tag{35}$$

Using the same transformations, the transformed boundary-conditions are

$$\overline{T}(X_1, X_2, s) = 10, \text{ for } (X_1, X_2) \in B_1, \tag{36}$$
$$\overline{T}(X_1, X_2, s) = \left(\frac{\frac{1}{s} + 30(0.814X_1 + 0.491X_2)^2 + 10}{s}\right), \text{ for } (X_1, X_2) \in B_2, \tag{37}$$
$$\frac{\partial \overline{T}(X_1, X_2, s)}{\partial n} = \left(\frac{\sqrt{\frac{k_1}{k}\left(\hat{X}_1\right)^2 + \frac{k_2}{k}\left(\hat{X}_2\right)^2}}{k\sqrt{\left(\hat{X}_1\right)^2 + \left(\hat{X}_2\right)^2}}\right) \times \left(\frac{-18(1.628X_1 - 0.245X_2)}{s^2}\right), \text{ for } (X_1, X_2) \in B_3, \tag{38}$$
$$\frac{\partial \overline{T}(X_1, X_2, s)}{\partial n} = \left(\frac{\sqrt{\frac{k_1}{k}\left(\hat{X}_1^*\right)^2 + \frac{k_2}{k}\left(\hat{X}_2^*\right)^2}}{k\sqrt{\left(\hat{X}_1^*\right)^2 + \left(\hat{X}_2^*\right)^2}}\right) \times \left(\left(\frac{18(1.628X_1 - 0.245X_2)}{s^2}\right) + \left(\frac{180(1.628X_1 - 0.245X_2) + 270}{s}\right)\right), \text{ for } (X_1, X_2) \in B_4. \tag{39}$$

To implement the DRBEM, curve B is discretized into 404 boundary elements, and 81 interior collocation points

are chosen. Some of numerical results obtained at selected points are presented and compared with the corresponding analytic solutions. The results are presented in Table I.

TABLE I: Comparison of numerical and analytical solutions of T at selected times and points

Time	(x_1, x_2)	Numerical	Exact	Abs. Error	% Error
$t = 1$	$(0.1, 0.1)$	10.03972	10.04	0.00028	0.003%
	$(0.5, 0.5)$	13.99766	14	0.00234	0.017%
	$(0.9, 0.9)$	32.67688	32.68	0.00312	0.009%
$t = 5$	$(0.1, 0.1)$	10.08028	10.08	0.00028	0.003%
	$(0.5, 0.5)$	14.99565	15	0.00435	0.029%
	$(0.9, 0.9)$	35.90988	35.92	0.01012	0.028%
$t = 10$	$(0.1, 0.1)$	10.13048	10.13	0.00048	0.005%
	$(0.5, 0.5)$	16.24273	16.25	0.00727	0.045%
	$(0.9, 0.9)$	39.95123	39.97	0.01877	0.047%

Table I shows a comparison of numerical solutions obtained using the DRBEM and corresponding analytic solutions at three selected points at three different times t. The three selected points are $(0.1, 0.1), (0.5, 0.5)$ and $(0.9, 0.9)$. From the results presented in Table I, it can be seen that as t increases, increases in the absolute errors are observed. For instance, at point $(0.1, 0.1)$ the absolute error at $t = 1$ is about 0.00028. The absolute error increases and reaches 0.00048 at $t = 10$. The other two points, $(0.5, 0.5)$ and $(0.9, 0.9)$, share the similar fashion.

Among the three points, numerical solutions at point $(0.1, 0.1)$ are the most accurate solutions. On the other hand, numerical solutions at $(0.9, 0.9)$ are less accurate compared to the numerical solutions at the other two points. Specifically, at $t = 5$, the absolute error of the numerical solution at $(0.1, 0.1)$ is about 0.00028, which is the most accurate compared to 0.00435 at $(0.5, 0.5)$ and 0.01012 at $(0.9, 0.9)$. The similar trends also occur at $t = 1$ and $t = 10$.

The percentages of error are also presented in Table I. As before, the percentages of error increase as t increases. For point $(0.1, 0.1)$ the percentage of error rises from 0.003% at $t = 1$ to 0.005% at $t = 10$. The rises in the percentage of error at $(0.5, 0.5)$ are observed from 0.0017% at $t = 1$ to 0.0045% at $t = 10$. A steep increase in the percentages of error occur at $(0.9, 0.9)$ from 0.0009% at $t = 1$ to 0.0047% at $t = 10$. Nevertheless, from the results presented, the numerical solutions obtained using the method are in a good accuracy.

B. Problem 2

In this problem, we consider a heat equation

$$1.7\frac{\partial^2 T}{\partial x_1^2} + 4.29\frac{\partial^2 T}{\partial x_2^2} - 0.24\frac{\partial^2 T}{\partial x_1 \partial x_2} + 18.08x_1 - 71.4x_2 + 326.04 = \frac{\partial T}{\partial t}, \quad (40)$$

subject to initial boundary conditions

$$T(x_1, x_2, 0) = 38x_2^2 + 21x_1^2 x_2 + 8 \quad (41)$$

$$T(x_1, x_2, t) = 38x_2^2 + 8, \text{ for } (x_1, x_2) \in B_1 \text{ and } t > 0, \quad (42)$$

$$T(x_2, x_2, t) = 38x_2^2 + 21x_2 + 8t + 8, \text{ for } (x_1, x_2) \in B_2 \text{ and } t > 0, \quad (43)$$

$$\sum_{i=1}^{2}\sum_{j=1}^{2} k_{ij}\frac{\partial T}{\partial x_i}n_{x_j} = -96.6x_1^2 + 0.96t, \text{ for } (x_1, x_2) \in B_3 \text{ and } t > 0, \quad (44)$$

$$\sum_{i=1}^{2}\sum_{j=1}^{2} k_{ij}\frac{\partial T}{\partial x_i}n_{x_j} = 96.6x_1^2 - 5.04x_1 - 0.96t + 326.04, \text{ for } (x_1, x_2) \in B_4 \text{ and } t > 0, \quad (45)$$

where B_1, B_2, B_3 and B_4 are defined as those in (24) - (27).

The analytic solution of the problem is

$$T(x_1, x_2, t) = 21x_1^2 x_2 + 38x_2^2 + 8tx_1 + 8. \quad (46)$$

As before, heat equation (40) is transformed into a Helmholtz-type equation using the set of transformations presented in the preceding section. Using the set of transformations, heat equation (40) can be written as

$$\begin{aligned}&\frac{\partial^2 \overline{T}}{\partial {X_1}^2} + \frac{\partial^2 \overline{T}}{\partial {X_2}^2} - \left(\frac{s}{k}\right)\overline{T} \\ &= \frac{1}{k}\Big[-21(0.6682X_1 - 0.2362X_2)^2(1.0824X_1 \\ &+ 0.4134X_2)^2 - 38(1.0824X_1 + 0.4134X_2)^2 - 8\Big] \\ &- \frac{1}{sk}\Big[(0.6682X_1 - 0.2362X_2)^2 - 180(0.6682X_1 \\ &- 0.2362X_2) - 120(0.1059X_1 + 1.4965X_2) - \frac{4}{s}\Big]. \quad (47)\end{aligned}$$

The transformed boundary-conditions are

$$\overline{T}(X_1, X_2, s) = \frac{38(0.106X_1 + 1.496X_2)^2 + 8}{s}, \text{ for } (X_1, X_2) \in B_1, \quad (48)$$

$$\overline{T}(X_1, X_2, s) = \frac{38(0.106X_1 + 1.496X_2)^2}{s} + 6\frac{21(0.106X_1 + 1.496X_2) + 8 + \frac{0.8}{s}}{s}, \text{ for } (X_1, X_2) \in B_2, \quad (49)$$

$$\frac{\partial \overline{T}(X_1, X_2, s)}{\partial n} = \left(\frac{\sqrt{\frac{k_1}{k}\left(\hat{X}_1\right)^2 + \frac{k_2}{k}\left(\hat{X}_2\right)^2}}{k\sqrt{\left(\hat{X}_1\right)^2 + \left(\hat{X}_2\right)^2}}\right) \times \left[\left(\frac{-105(0.668X_1 - 0.236X_2)^2}{s}\right) + \frac{0.8}{s^2}\right], \text{ for } (X_1, X_2) \in B_3, \quad (50)$$

$$\frac{\partial \overline{T}(X_1, X_2, s)}{\partial n} = \left(\frac{\sqrt{\frac{k_1}{k}\left(\hat{X}_1^*\right)^2 + \frac{k_2}{k}\left(\hat{X}_2^*\right)^2}}{k\sqrt{\left(\hat{X}_1^*\right)^2 + \left(\hat{X}_2^*\right)^2}}\right)$$

$$\times \left[\left(\frac{105(0.668X_1 - 0.236X_2)^2}{s} \right) - \left(\frac{4.2(0.668X_1 - 0.236X_2) + 380}{s} \right) - \frac{0.8}{s^2} \right], \text{ for } (X_1, X_2) \in B_4, \quad (51)$$

After performing several computational experiments, it is obtained that a good accuracy and efficiency achieved when the boundary is discretized into 410 elements, and 81 interior collocation points are chosen. Some of the results obtained are presented in Figure 2 and Figure 3.

Figure 2 shows graphs of numerical solutions and the corresponding analytical solutions along selected lines at various time t. More specifically, the selected lines are $x_1 = 0.2$, $x_1 = 0.5$, and $x_1 = 0.8$. The times t presented in the graphs are $t = 1$, $t = 5$, and $t = 10$. It can be seen from Figure 2 that the graphs of numerical solutions and the corresponding analytical solutions coincide. This means that numerical solutions obtained using the method are in a good accuracy. This shows that the numerical method presented in the preceding section is a suitable method for solving the problem numerically.

Figure 3 shows the percentage of errors of the numerical solutions of the problem along the selected lines and times t as those in Figure 2. From Figure 3, we can observe that the percentage of errors of numerical solutions are less than 0.2%. We can also observe that the percentages of error tend to increase as t rises. For more specific discussion, at $t = 1$ (Figure 3(a)), it can be seen that the percentage of error tends to decrease as x_2 increases. Along line $x_1 = 0.2$, the percentage of error is ranged between 0.01% and 0.07%. Values of the percentage of error along line $x_1 = 0.5$ are between 0.02% and 0.08%. Along $x_1 = 0.8$, the percentage of errors is arranged between 0.03% and 0.1%. It is examined that at any value of x_2, except at $x_2 = 0.7$, the percentage of error at $x_1 = 0.2$ is the smallest. On the other hand, at $x_1 = 0.8$, the percentage of error is the highest.

For $t = 5$ and $t = 10$, the graphs of the percentages of error are shown in Figure 3(b) and Figure 3(c), respectively. From the figures, the graphs of percentage of error have similar fashion as those at $t = 1$. For $t = 5$, along line $x_1 = 0.2$, the percentage of error are between 0.04% and 0.13%. The percentages of error along line $x_1 = 0.5$ and $x_1 = 0.8$ are from 0.07% to 0.15% and from 0.09% to 0.17%, respectively. For $t = 10$, the percentages of error along $x_1 = 0.2$, $x_1 = 0.5$, and $x_1 = 0.8$ are ranged between 0.07% to 0.16%, 0.1% to 0.18%, and 0.12% to 0.19%, respectively. As before, the results show that the numerical method used gives numerical solutions with high accuracy.

C. Problem 3

In the previous two problems, analytical solutions of the problems are known. Hence, the numerical solutions obtained can be compared with the corresponding analytical solutions to investigate accuracy of the method. From the results presented and discussed, it can be concluded that numerical solutions obtained using the method presented are in good accuracy. Hence, the method may be applied to solve heat equation problems in anisotropic materials numerically.

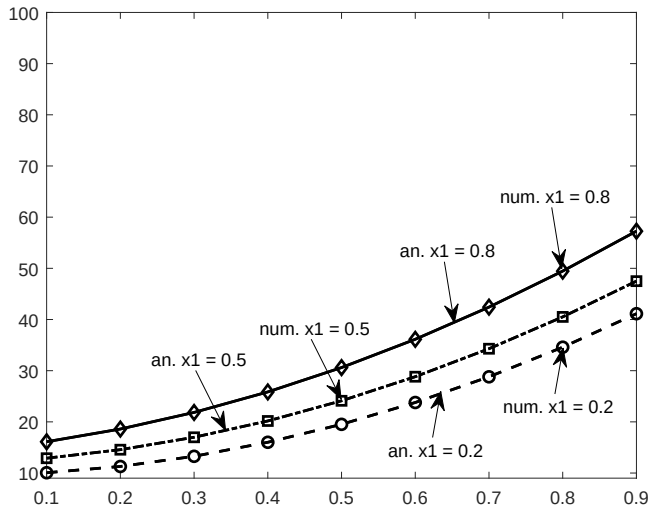

(a) $t = 1$

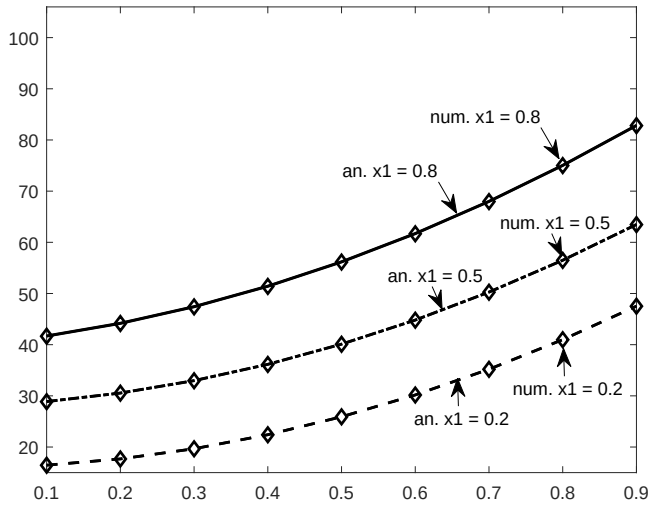

(b) $t = 5$

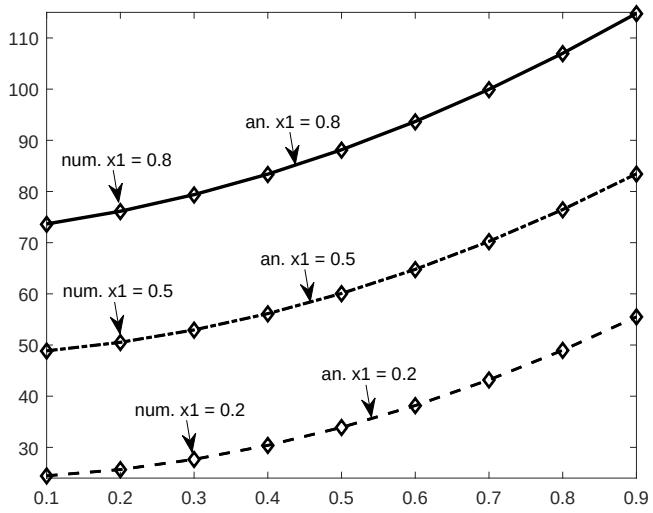

(c) $t = 10$

Fig. 2: Numerical and analytic solutions along selected values of x_1 at various t.

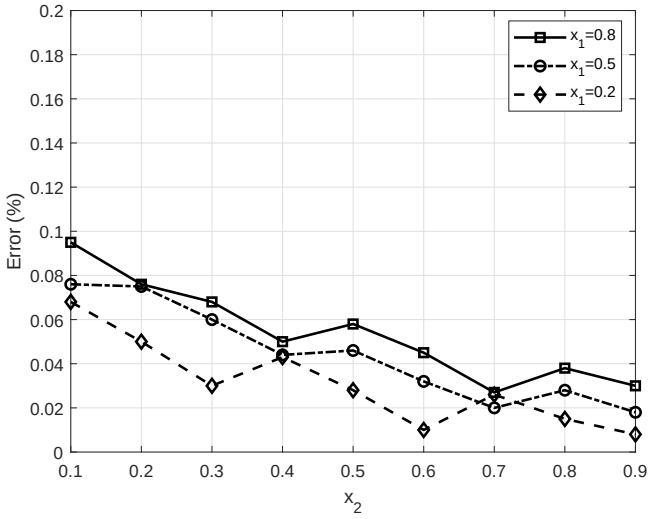

(a) $t = 1$

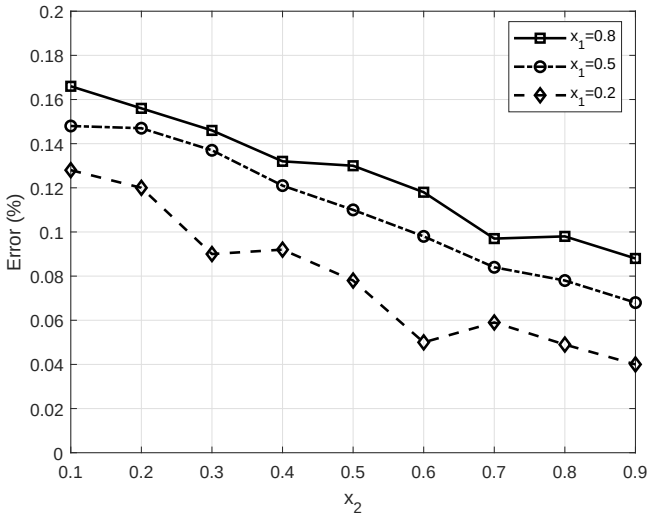

(b) $t = 5$

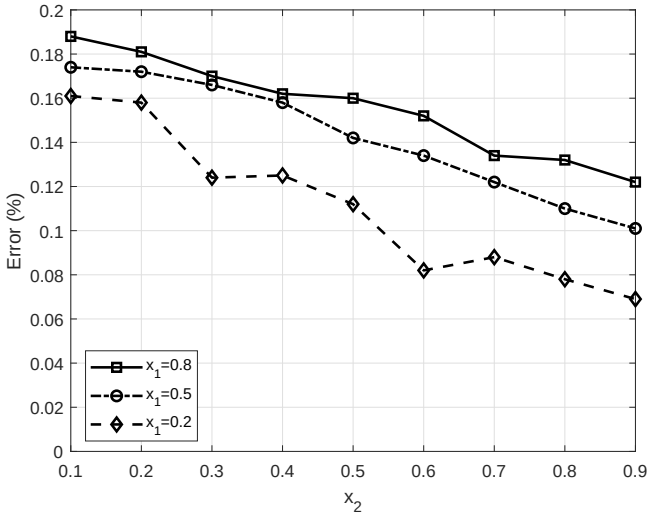

(c) $t = 10$

Fig. 3: Percentage errors along selected values of x_1 at various t.

In Problem 3, we consider a problem with unknown analytic solution. The problem is governed by equation

$$1.7\frac{\partial^2 T}{\partial x_1^2} + 4.29\frac{\partial^2 T}{\partial x_2^2} - 0.24\frac{\partial^2 T}{\partial x_1 \partial x_2} = \frac{\partial T}{\partial t}, \tag{52}$$

subject to initial and boundary conditions

$$T(x_1, x_2, 0) = 0 \tag{53}$$

$$T(x_1, x_2, t) = 100, \text{ for } (x_1, x_2) \in B_1 \text{ and } t > 0, \tag{54}$$

$$T(x_2, x_2, t) = 30, \text{ for } (x_1, x_2) \in B_2 \text{ and } t > 0, \tag{55}$$

$$\sum_{i=1}^{2}\sum_{j=1}^{2} k_{ij}\frac{\partial T}{\partial x_i}n_{x_j} = 0, \text{ for } (x_1, x_2) \in B_3 \text{ and } t > 0, \tag{56}$$

$$\sum_{i=1}^{2}\sum_{j=1}^{2} k_{ij}\frac{\partial T}{\partial x_i}n_{x_j} = 0, \text{ for } (x_1, x_2) \in B_4 \text{ and } t > 0, \tag{57}$$

where B_1, B_2, B_3, and B_4 are as those in (24) - (27).

To solve the problem numerically, the governing equation is transformed into a Helmholtz-type equation

$$\frac{\partial^2 \overline{T}}{\partial {X_1}^2} + \frac{\partial^2 \overline{T}}{\partial {X_2}^2} - \left(\frac{s}{k}\right)\overline{T} = 0. \tag{58}$$

The transformed boundary-conditions are

$$\overline{T}(X_1, X_2, s) = \frac{100}{s}, \text{ for } (X_1, X_2) \in B_1, \tag{59}$$

$$\overline{T}(X_1, X_2, s) = \frac{30}{s}, \text{ for } (X_1, X_2) \in B_2, \tag{60}$$

$$\frac{\partial \overline{T}(X_1, X_2, s)}{\partial n} = 0, \text{ for } (X_1, X_2) \in B_3, \tag{61}$$

$$\frac{\partial \overline{T}(X_1, X_2, s)}{\partial n} = 0, \text{ for } (X_1, X_2) \in B_4. \tag{62}$$

As that in Problem 2, the boundary B is discretized into 410 elements, and 81 interior collocation points are chosen. Some of numerical solutions obtained are presented in Figures 4 - 6.

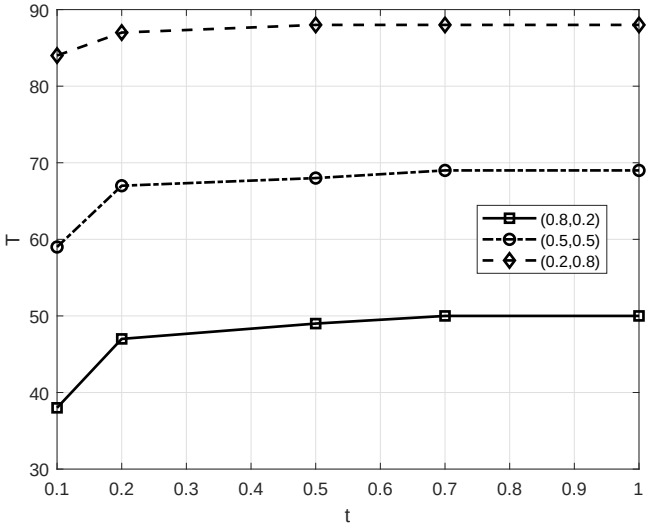

Fig. 4: Variation of temperature T at some points as time t increases.

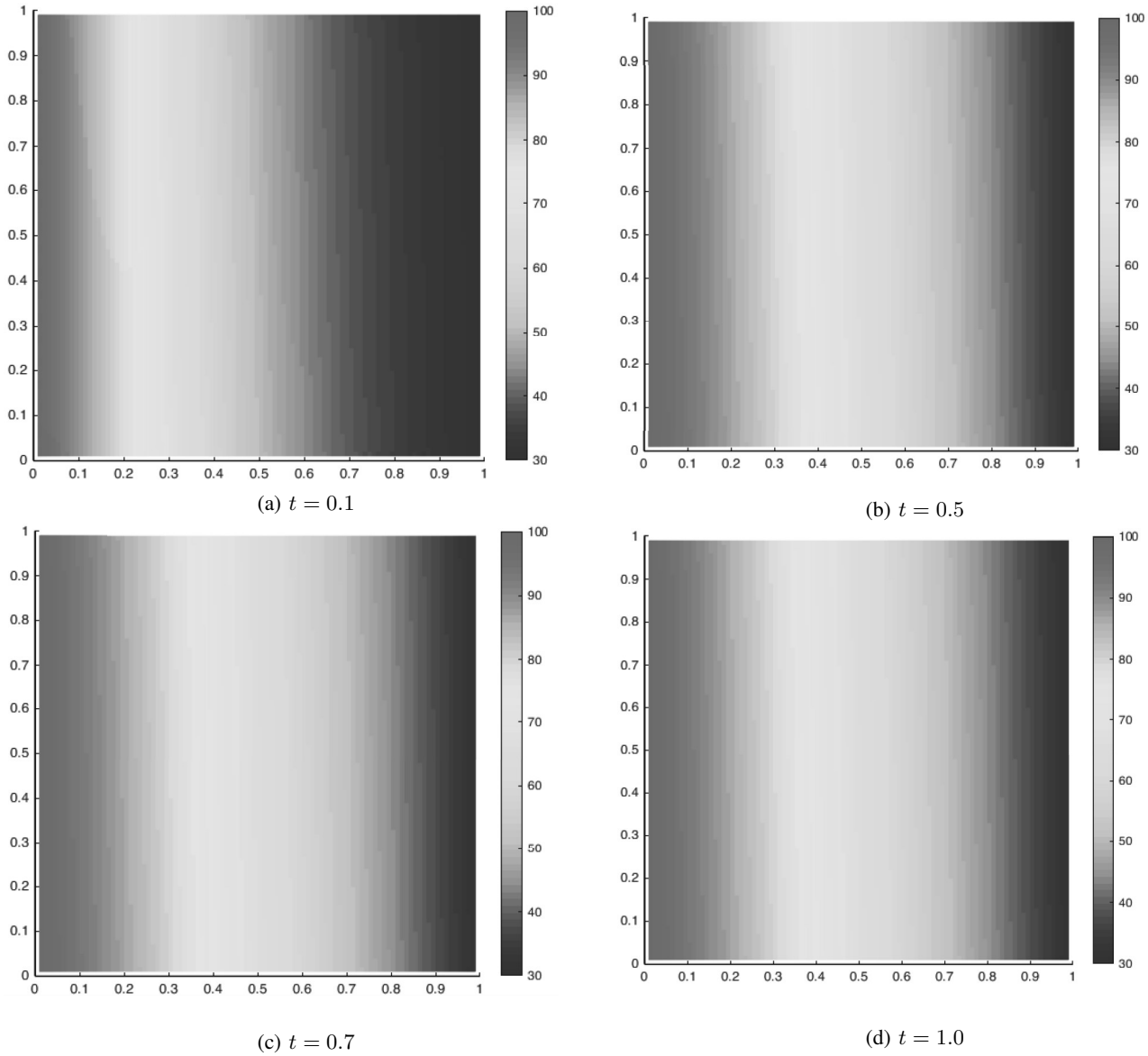

(a) $t = 0.1$

(b) $t = 0.5$

(c) $t = 0.7$

(d) $t = 1.0$

Fig. 5: Surface plot of temperature T over the region at four different times t.

Figure 4 shows the variation of the values of T at points $(0.2, 0.8)$, $(0.5, 0.5)$, and $(0.8, 0.2)$, from $t = 0.1$ to $t = 1$. It can be seen that at any time t, the temperature at point $(0.2, 0.8)$ is the highest compared to those at $(0.5, 0.5)$ and $(0.8, 0.2)$. On the other hand, the temperature at point $(0.8, 0.2)$ is the smallest contrasted to those at $(0.2, 0.8)$ and $(0.5, 0.5)$. These results are expected, as point $(0.2, 0.8)$ is the nearest point to line $x_1 = 0$, where the temperature on the line is the highest over the region, which is $100°$. On the other hand, point $(0.8, 0.2)$ is the furthest point to the line.

It can be observed that variations of T at the three different points have similar fashion. Specifically, at $(0.8, 0.2)$, temperature T increase steeply from about $38°$ at $t = 0.1$ to 47^o at $t = 0.2$. From $t = 0.2$ to $t = 0.5$, the temperature rise gradually from about $47°$ to $49°$. Gradual increase in temperature is still observed from $49°$ at $t = 0.5$ to $50°$ at $t = 0.7$, from which temperature reaches steady state situation. At $(0.5, 0.5)$ and $(0.2, 0.8)$, from $t = 0.1$ to $t = 0.2$ temperature T inclines from about $59°$ to $67°$ and from about $84°$ to $87°$, respectively. From $t = 0.2$ to $t = 0.5$, T rises gently from about $67°$ to $68°$ and from about $87°$ to $88°$, respectively. Especially for $(0.2, 0.8)$, T reaches its steady state situation at $t = 0.5$. For point $(0.5, 0.5)$, T increases slowly from 68^o to 69^o, from $t = 0.5$ to $t = 0.7$. At $t = 0.7$, it seems that the temperature at $(0.5, 0.5)$ has reach its steady state situation. Moreover, the rise in T at points nearer line $x_1 = 0$ is lower than those at further location. For instance, the rise in T from $t = 0.1$ to $t = 0.2$ at point $(0.8, 0.2)$, the furthest location from $x_1 = 0$ among the three points considered, is about 9^o. On the other hand, at point $(0.2, 0.8)$, the nearest location from $x_1 = 0$ among the three points examined, the increment in T is about $3°$.

Figure 5 shows surface plots of T over the region at four different times t. Specifically, Figure 5(a) shows surface plot of T at $t = 0.1$. Surface plot of T at $t = 0.5$ is shown in Figure 5(b). For $t = 0.7$ and $t = 1.0$, the surface plot of T are presented in Figure 5(c) and Figure 5(d), respectively. From Figure 5, it seems that there is no variational value in temperature T along any lines parallel to x_2 axis. Meanwhile, along any lines parallel to x_1 axis, variational of T is observed. It can also be observed that there is a big change in the distribution od T over the region from $t = 0.1$ to

$t = 0.5$. This means that there is observable increase in T over the region from $t = 0.1$ to $t = 0.5$. However, from $t = 0.5$ onwards, the distributions of T over the region are about the same. This result shows that at $t = 0.5$, the steady state condition is almost reached.

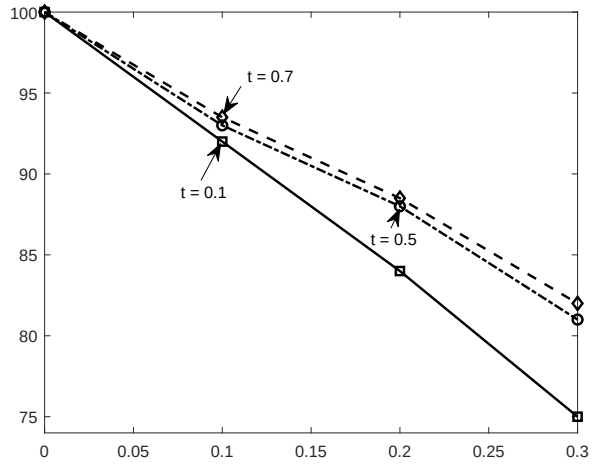

(a) $x_1 = 0$ to $x_1 = 0.3$

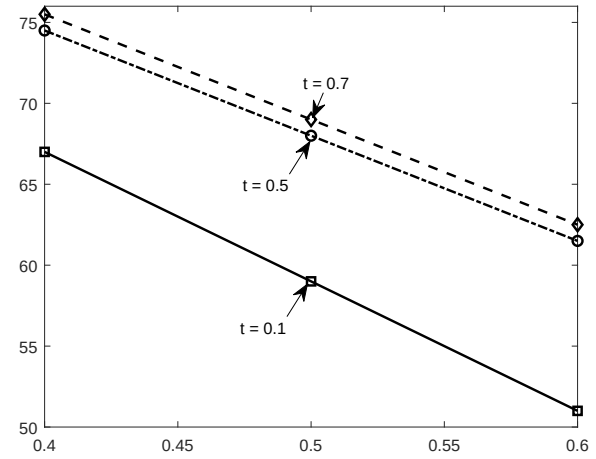

(b) $x_1 = 0.4$ to $x_1 = 0.6$

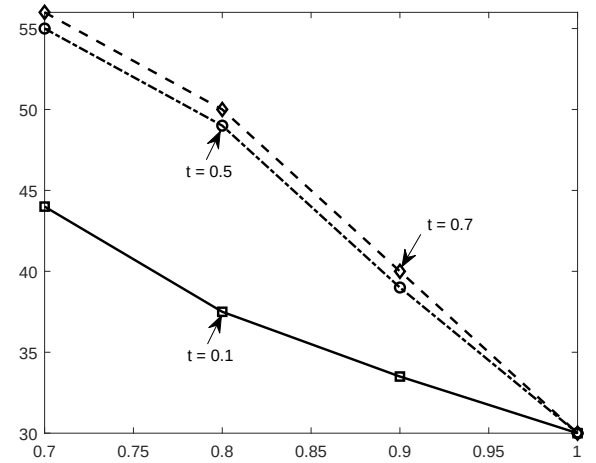

(c) $x_1 = 0.7$ to $x_1 = 1.0$

Fig. 6: Values of temperature T along x_1-axis for different times t.

From the surface plots presented (see Figure 5), it can be seen that for any time, the changes in T are observed along x-axis direction. Figure 6 shows values of T at any line $y = c$, $0 \leq c \leq 1$, for different times t. More specifically, there are four different times t, namely $t = 0.1$, $t = 0.5$, $t = 0.7$, and $t = 1.0$. In Figure 6, values of T at $t = 1.0$ are about the same as those at $t = 0.7$ (see Figure 4). Hence, the graph of T for $t = 1.0$ is the same as that for $t = 0.7$.

For any time t, temperature T decreases along x_1-axis. The decrease in T varies with times t. At $t = 0.1$, a steep decrease in T is observed from $x_1 = 0$ to $x_1 = 0.6$. Temperature T declines from 100° to about 50°. From $x_1 = 0.6$, T decreases gradually from about 50° to 30°. On the other hand, at $t = 0.5$, temperature $T = 50^\circ$ is achieved at $x_1 = 0.8$, from which temperature T drops significantly from 50° to 30° at $x_1 = 1$. At $t = 0.7$ and $t = 1.0$ (the graphs of T of these two t are coincide), small changes in the graph of T are detected, compared to that at $t = 0.5$. The values of T at $t = 0.7$ and $t = 1.0$ are about 0 to 2° higher than those at $t = 0.5$. These results show that major changes in the distribution of temperature T occurs from $t = 0.1$ to $t = 0.5$. From $t = 0.5$ to $t = 1$, small changes in T are observed. Moreover, it seems that the steady state has been achieved at $t = 0.7$.

IV. Concluding Remarks

Problems involving time-dependent heat distribution in anisotropic thin plates are considered. The problems are solved numerically using an LTDRM. In order to solve the problems using the LTDRM, a set of transformations involving coordinate transformations and a Laplace transform is employed to transform the governing equations into Helmholtz-type equations. The LTDRM is tested using two problems with analytic solution to examine its accuracy. The numerical results show that the method is a suitable and accurate method for solving the two problems, with percentage errors less than 0.2%.

The implementation of the DRBEM to solve Problem 3, a problem with unknown analytical solution, results in variational increase in temperature T at three different points. A point near the boundary with the highest temperature, a point in the middle of the plate, and a point near the boundary with lowest temperature. At the point near the highest temperature side of the thin plate, the increase in the temperature from one time to another time is smaller than those at further locations. On the other hand, at the point near the boundary with lowest temperature, the incline in the temperature is higher than those at other locations. Moreover, at the beginning, for instance from $t = 0.1$ to $t = 0.2$, sharp increases are observed over the region. After some times, for instance from $t = 0.5$ to $t = 0.7$, the distributions of temperature over the region are about the same. From the results presented, the steady state condition has been attained at $t = 0.7$.

References

[1] C. A. Paddock and G. L. Eesley,"Transient thermoreflectance from thin metal films," *J. Appl. Phys.*, vol. 60(1), pp. 285 - 290, 1986.

[2] W. S. Capinski, H. J. Maris, T. Ruf, M. Cardona, K. Ploog, and D. S. Katzer, "Thermal-conductivity measurements of GaAs/AlAs superlattices using a picosecond optical pump-and-probe technique," *Phys. Rev. B*, vol. 59(12), pp. 8105 - 8113, 1999.

[3] P. M. Norris, A. P. Caffrey, R. J. Stevens, J. M. Klopf, J. James, T. McLeskey, and A. N. Smith, "Femtosecond pump–probe nondestructive examination of materials," *Rev. Sci. Instrum.*, vol. 74(1), pp. 400 - 406, 2003.
[4] S. Huxtable, D. G. Cahill, V. Fauconnier, J. O. White, and J. C. Zhao, "Thermal conductivity imaging at micrometre-scale resolution for combinatorial studies of materials," *Nature Mater.*, vol. 3, pp. 298 - 301, 2004.
[5] D. L. Clements, and M. Lobo, "A BEM for Time Dependent Infiltration from an Irrigation Channel," Engineering Analysis with Boundary Elements, vol. 34, pp. 1100 – 1104, 2010.
[6] I. Solekhudin, "A Numerical Method for Time-Dependent Infiltration from Periodic Trapezoidal Channels with Different Types of Root-Water Uptake," IAENG International Journal of Applied Mathematics, vol. 48 no. 1, pp. 84 - 89, 2018.
[7] Munadi, I. Solekhudin, Sumardi, A. Zulijanto, "Steady water flow from different types of single irrigation channel," JP Journal of Heat and Mass Transfer, vol. 16 no. 1, pp. 95 – 106, 2019.
[8] Munadi, I. Solekhudin, Sumardi, and A. Zulijanto, "A Numerical Study of Steady Infiltration from a Single Irrigation Channel with an Impermeable Soil Layer," Engineering Letters, vol. 28 no. 3, pp. 643 – 650, 2020.
[9] N. Y. Ashar, and I. Solekhudin, "A Numerical Study of Steady Pollutant Spread in Water from a Point Source," Engineering Letters, vol. 29 no. 3, pp. 840 – 848, 2021.
[10] I. Solekhudin, "Boundary interface water infiltration into layered soils using dual reciprocity methods," Engineering Analysis with Boundary Elements, vol. 119, pp. 280 – 292, 2020.
[11] W. T. Ang, and D. L. Clements, "Nonlinear Heat Equation for Nonhomogeneous Anisotropic Materials: A Dual-Reciprocity Boundary Element Solution," Numerical Methods for Partial Differential Equations, vol. 26, pp. 771-784, 2009.
[12] M. I. Azis, I. Solekhudin, M. H. Aswad, S. Hamzah, and A. R. Jalil, "A Combined Laplace Transform and Boundary Element Method for Unsteady Laplace Problems of Several Classes of Anisotropic Functionally Graded Materials," Engineering Letters, vol. 29 no. 2, pp. 534 - 542, 2021.
[13] I. Solekhudin, "Suction potential and water absorption from periodic channels in a homogeneous soil with different root uptakes," Advances and Applications in Fluid Mechanics, vol. 20 no. 1, pp. 127 – 139, 2017.
[14] I. Solekhudin, D. Purnama, N. H. Malysa, and Sumardi, "Characteristic of Water Flow in Heterogeneous Soils" JP Journal of Heat and Mass Transform, vol. 15 no. 3, pp. 597 – 608, 2018.
[15] H. Stehfest, "Numerical Inversion of Laplace Transform," *Communication of the ACM*, vol. 13(1), pp. 47 - 54, 1968.